Preprints of the 3rd IFAC Conference on Advances in Proportional-
Integral-Derivative Control, Ghent, Belgium, May 9-11, 2018

ThAT2.4

Robust Tuning Rules for Series Elastic Actuator PID Cascade Controllers

Stefano Ghidini * Manuel Beschi * Nicola Pedrocchi *
Antonio Visioli **

* *Institute of Industrial Technologies and Automation, National Research Council of Italy, Via Corti 12, 20133, Milan, Italy (e-mail: stefano.ghidini,manuel.beschi,nicola.pedrocchi@itia.cnr.it)*
** *Department of Mechanical and Industrial Engineering, University of Brescia, Via Branze 38, 25123 Brescia, Italy (e-mail: antonio.visioli@unibs.it)*

Abstract: This paper deals with the control of a collaborative robot manipulator with series elastic actuators. In particular, robust tuning rules for cascade control of the joints are presented. Both the motor velocity and link position control loops are considered. The proposed tuning rules allow the online computation of robust control parameters to cope with the different link reflected inertia. Experimental results show the effectiveness of the method in real applications.

Keywords: Collaborative robots; Series elastic actuator; Robust control; PID; Tuning rules.

1. INTRODUCTION

Standard industrial robots are not typically designed to co-exist with humans in the same working environment. In fact, industrial robots are usually employed in several tasks in an isolated workspace by means of walls or fences. They are designed to provide high accuracy and precision, but the achievement of such a high level performance makes them characterized by a rigid and heavy structure. These features do not allow robots to reach the safety conditions that are necessary to share a working environment with humans without expensive tools like sensitive skin.

Due to the increased demand of human-robot interaction, a paradigm shift is changing the structural design of the robot to reduce the impact forces during possible collision. In recent years, a class of lightweight industrial robot has been presented (Guiochet et al., 2017) where the impact forces are reduced by limiting the mass, and therefore the momentum of the robot, and the maximum exerted forces. However, many tasks do not require the precision provided by an industrial robot and therefore impact forces reduction can be obtained by introducing elastic elements in the robot chain (Verstraten et al., 2016). Series Elastic Actuators (SEAs) are explicitly designed to pursue this idea. In fact, an elastic element is inserted in series to the actuator thus reducing the part of the mass that directly impacts the human, and therefore the overall impact force. Moreover, springs allow estimating the exerted forces without the use of expensive force/torque sensors. However, this type of structure makes the control of the link position more difficult (Maleki et al., 2016; Paine et al., 2014; Ragonesi et al., 2011; Calanca and Fiorini, 2017; Calanca et al., 2017; Dos Santos and Siqueira, 2014). Indeed, the actual position of the link is given by the position of the gearbox output shaft plus the spring deformation. The elasticity implies the presence of a resonance and antiresonance behavior in the frequency response, coupled with the typical small damping factor of metallic spring elements. Moreover, there are multiple sources of

model mismatches: the reflected inertia strongly depends on the robot configuration and on the (possibly unknown) payload. Further, the spring characteristic can be non-linear, aging can increase hysteresis and backlash, static and viscous friction terms strongly depend on temperature (Simoni et al., 2017), and the rigid body assumption could not be an accurate hypothesis for lightweight links.

Those model mismatches can imply significant detriment in model-based control strategies which do not take them into account. In this case, it is reasonable to employ a robust PID-based control architecture instead of an adaptive model-based algorithm. One limit of this solution is the computational burden of an *ad-hoc* robust tuning optimization, which is not compatible with modular design (Maurtua et al., 2016). In fact, the robot presents a modular design, thus its overall inertia may change based on the setup of the mechanical structure. Moreover, in many applications, the usage of a single controller for the entire robot workspace can lead to very poor performance, requiring the retuning of the controllers. In this case, a gain-scheduling approach is proven to be an effective solution. Also in this case, effective robust tuning rules can be used to tune the controller without the need of an external dedicated computer (Misgeld et al., 2017).

The approximation of robust problem solutions with tuning rules is a common strategy in process control (Åström and Hägglund, 2004), but there are no tuning rules that address the control of elastic mechanical systems, as far as the authors know. The aim of this paper is to cope with this issue by proposing robust tuning rules for series elastic actuators. In this way, it is possible to guarantee a robust performance by limiting the maximum sensitivity in link position and motor velocity controllers for different values of the reflected inertia and different damping levels.

The paper is organized as follows: in Section 2 is described the dynamic model of the the SEA. In Section 3 is proposed the optimization problem performed to obtain specific tuning rules, able to guarantee robust performance.
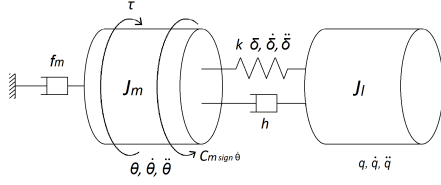
Fig. 1. Illustrative scheme of the SEA model.

The experimental results are described in Section 4 , they
have been obtained by means of two trajectories on a three
degree-of-freedom series elastic actuated robot.

2. SERIES ELASTIC ACTUATOR MODEL

A series elastic actuator manipulator can be modeled
as an open kinematic chain consisting of a rigid link
and lumped elastic part coaxial with the joint rotational
axis. The proposed approach considers a decentralized
model, where the coupling effects are considered as model
mismatches. This model takes into account two inertias:
the first one represents the motor and the gearbox, while
the second one represents the inertia of the link and of
the downstream part of the kinematic chain for the actual
joint configuration. Thus, the state variables are the motor
position θ, the motor velocity $\dot{\theta}$, the spring deflection δ and
the spring velocity $\dot{\delta}$. Other interesting variables are the
link position $q = \theta + \delta$ and its velocity $\dot{q} = \dot{\theta} + \dot{\delta}$, which
represent the real motion of the link. A joint model can be
derived by dynamic laws as:

$$\begin{cases} J_m \ddot{\theta} = h\dot{\delta} + k\delta - f_m\dot{\theta} + \tau - C_m \operatorname{sign} \dot{\theta} \\ J_l(\ddot{\theta} + \ddot{\delta}) = -h\dot{\delta} - k\delta \end{cases} \quad (1)$$

where J_m is the motor inertia, J_l is the link (and the
downstream part of the kinematic chain) inertia, τ is the
motor torque, f_m is the motor viscous friction (between
motor and stator), C_m is the motor Coulomb friction
(between motor and stator), k is the elasticity (between
link and motor), and h is the viscosity (between link and
motor). An illustrative scheme of the model is shown in
Figure 1.
Equation (1) can be linearized by neglecting the Coulomb
friction terms, so that the resulting transfer function
between the motor torque and the motor velocity is:

$$P_{\dot{\theta},\tau}(s) = \frac{\dot{\theta}(s)}{\tau(s)} =$$
$$\frac{J_l s^2 + hs + k}{J_l J_m s^3 + (J_l f_m + (J_m + J_l)h)s^2 + ((J_l + J_m)k + f_m h)s + f_m k} \quad (2)$$

while the transfer function between the motor torque and
the link position is:

$$P_{q,\tau}(s) = \frac{q(s)}{\tau(s)} =$$
$$\frac{hs + k}{(J_l J_m s^3 + (J_l f_m + (J_m + J_l)h)s^2 + ((J_l + J_m)k + f_m h)s + f_m k)s} \quad (3)$$

It is worth stressing that the link inertia J_l strongly
depends on the robot configuration and on the (possi-
bly unknown) payload, while several possible model mis-
matches can occur in real setup. For example, the spring
characteristic can be nonlinear, and aging can increase
hysteresis and backlash. Finally, static and viscous fric-
tion terms might strongly depend on temperature (Simoni
et al., 2017). Those model mismatches can imply signifi-
cant detriment in model-based control strategies which do
not take them into account.
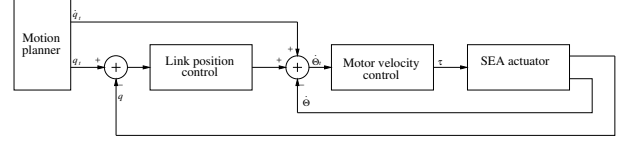
Fig. 2. Cascade control scheme.

A robust cascade controller is therefore used to cope with
mismatches without complex model adaptivity algorithms.
The primary loop regulates the link position by acting on
the motor velocity set-point $\dot{\theta}_{sp}$, that is the input of the
secondary loop, which computes the desired torque. The
current loop is considered fast enough to be neglected.
Figure 2 shows the overall scheme.

2.1 Reduction of model parameters

In order to simplify the robust tuning rules expression, a
model similarity is used to reduce the number of model
parameters.
Rewriting (1) in the Laplace domain it is possible to
obtain:

$$J_m s^2 \theta = hs\delta + k\delta - f_m s\theta + \tau \quad (4)$$
$$J_l s^2(\theta + \delta) = -hs\delta - k\delta \quad (5)$$

Then, by defining the following quantities

$$s = \sqrt{\frac{k}{J_m}}\hat{s} \Leftrightarrow \hat{s} = \sqrt{\frac{J_m}{k}}s,$$
$$\hat{\theta} = k\theta \qquad \hat{\delta} = k\delta, \quad \hat{J}_l = \frac{J_l}{J_m},$$
$$\hat{f}_m = \frac{f_m}{k}\sqrt{\frac{k}{J_m}}, \quad \hat{h} = \frac{h}{k}\sqrt{\frac{k}{J_m}} \quad (6)$$

it is possible to rewrite (4) as

$$\hat{s}^2\hat{\theta} = \hat{h}\hat{s}\hat{\delta} + \hat{\delta} - \hat{f}_m\hat{s}\hat{\theta} + \tau \quad (7)$$

and (5) as

$$\hat{J}_l\hat{s}^2(\hat{\theta} + \hat{\delta}) = -\hat{h}\hat{s}\hat{\delta} - \hat{\delta} \quad (8)$$

The ratio $\hat{J}_l$ is the most important parameter, in fact,
it causes a decrement of the resonance and antiresonance
frequencies as shown in Figure 3 and, at the same time, it
increases their peaks. The effect of $\hat{h}$, shown in Figure 4, is
mainly on resonance and antiresonance peaks, while their
frequencies present a slight shift. Finally, the motor viscous
friction parameter changes the low frequency behavior and
it reduces the resonance peak.
It is worth stressing that $\hat{h}$ has normally a small value
for mechanical elastic elements (like torsional, coned-disc
and coil springs) without dampers, while $\hat{f}_m$ has not
a significant impact on the crossover frequency range.
Finally, it is important to note that the motor velocity
frequency response is less sensible to parameter changes
for frequencies higher than the resonance frequency.

3. ROBUST OPTIMAL TUNING

The tuning procedure starts by considering the inner loop
and continues with the outer one. The process of the inner
loop has a transfer function defined between τ and $\dot{\theta}$. Once
the tuning parameters of this loop have been detected, the
velocity closed loop obtained will be seen as the process
of the outer loop, which has a transfer function defined
between $\dot{\theta}$ and q.
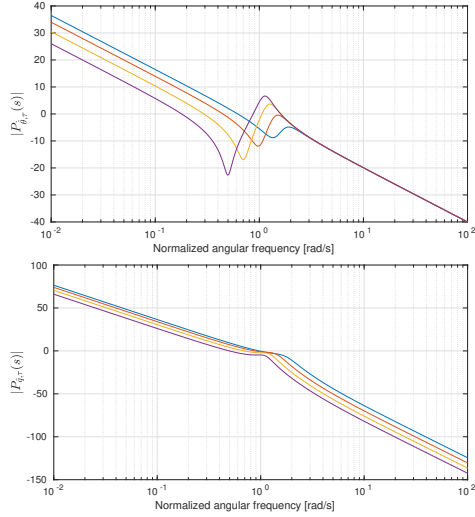
Fig. 3. Effect of the parameter $\hat{J}_l$ on frequency responses $P_{\dot{\hat{\theta}},\tau}(s)$ (upper plot), $P_{\hat{q},\tau}(s)$ (lower plot). Blue line: $\hat{J}_l = 0.5$, $\hat{h} = 0.2$, $\hat{f}_m = 0$. Magenta line: $\hat{J}_l = 1$, $\hat{h} = 0.2$, $\hat{f}_m = 0$. Ocher line: $\hat{J}_l = 2$, $\hat{h} = 0.2$, $\hat{f}_m = 0$. Violet line: $\hat{J}_l = 4$, $\hat{h} = 0.2$, $\hat{f}_m = 0$.
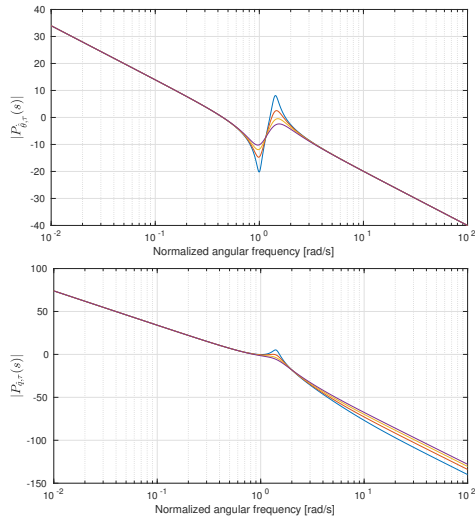
Fig. 4. Effect of the parameter $\hat{h}$ on frequency responses $P_{\dot{\hat{\theta}},\tau}(s)$ (upper plot), $P_{\hat{q},\tau}(s)$ (lower plot). Blue line: $\hat{J}_l = 1$, $\hat{h} = 0.1$, $\hat{f}_m = 0$. Magenta line: $\hat{J}_l = 1$, $\hat{h} = 0.2$, $\hat{f}_m = 0$. Ocher line: $\hat{J}_l = 1$, $\hat{h} = 0.3$, $\hat{f}_m = 0$. Violet line: $\hat{J}_l = 1$, $\hat{h} = 0.4$, $\hat{f}_m = 0$.

3.1 Motor velocity control

A PI controller regulates the motor torque to reduce the speed trajectory error. The controller is described by the following transfer function:

$$C_v(s) = K_{p,v} + \frac{K_{i,v}}{s} \tag{9}$$

where $K_{p,v}$ is the proportional gain and $K_{i,v}$ is the integral gain. The controller parameters can be rewritten by following (6) as
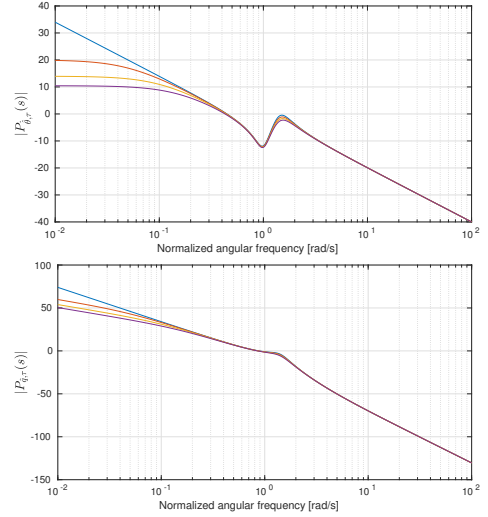
Fig. 5. Effect of the parameter $\hat{f}_m$ on frequency responses $P_{\dot{\hat{\theta}},\tau}(s)$ (upper plot), $P_{\hat{q},\tau}(s)$ (lower plot). Blue line: $\hat{J}_l = 1$, $\hat{h} = 0.3$, $\hat{f}_m = 0$. Magenta line: $\hat{J}_l = 1$, $\hat{h} = 0.3$, $\hat{f}_m = 0.1$. Ocher line: $\hat{J}_l = 1$, $\hat{h} = 0.3$, $\hat{f}_m = 0.2$. Violet line: $\hat{J}_l = 1$, $\hat{h} = 0.3$, $\hat{f}_m = 0.3$.

$$\hat{K}_{p,v} = K_{p,v} \frac{\sqrt{k/J_m}}{k}, \quad K_{p,v} = \hat{K}_{p,v} \frac{k}{\sqrt{k/J_m}},$$
$$\hat{K}_{i,v} = K_{i,v} \frac{1}{k}, \qquad K_{i,v} = \hat{K}_{i,v} k, \tag{10}$$

The controller parameters are then computed by solving the following optimization problem:

$$\min (\hat{\omega}_{c,v} - \hat{\omega}_{d,v})^2 - \lambda_v \phi_m$$

$$\text{subject to:} \begin{cases} \phi_m \geq \phi_{m,min} \\ M_s \leq M_{s,max} \\ |L_v(\hat{\omega})| \leq L_{h,v,max}, & \text{if } \hat{\omega} \geq \hat{\omega}_h \\ |L_v(\hat{\omega})| \geq L_{l,v,min}, & \text{if } \hat{\omega} \leq \hat{\omega}_l \end{cases} \tag{11}$$

where $\hat{\omega}$ is the normalized angular frequency, $\hat{\omega}_{c,v}$ and $\hat{\omega}_{d,v}$ are, respectively, the cutoff frequency and its desired value, $\lambda_v > 0$ is a weighting factor, ϕ_m and M_s are the phase margin and the maximum sensitivity, $L_v(\hat{\omega}) = C_v(\hat{\omega}) P_{\dot{\hat{\theta}},\tau}(\hat{\omega})$ is the loop transfer function, $L_{h,v,max}$ is the maximum allowed value of $|L(\hat{\omega})|$ for frequencies greater than $\hat{\omega}_h$, and $L_{l,v,min}$ is the minimum allowed value for frequencies lower than $\hat{\omega}_l$. In the tuning procedure, those values has been set equal to:

$$\begin{array}{ll} L_{h,v,max} = -40dB, & \hat{\omega}_h = 100\hat{\omega}_d, \\ L_{l,v,min} = 40dB, & \hat{\omega}_h = 0.01\hat{\omega}_d, \\ M_{s,max} = 1.4, & \phi_{m,min} = 60° \\ \lambda_v = 10^{-2} \end{array} \tag{12}$$

It is worth stressing that the presence of the antiresonance zeros can cause multiple crossing of the 0dB axis, and therefore the system has more than one phase margin. In this case, the most critical value is taken into account in the optimization algorithm. Due to these multiple cutoff frequencies, the maximum sensitivity M_s is therefore of utmost importance to guarantee the required level of robustness. The term $-\lambda \phi_m$ of the cost function discerns between solutions with the same cutoff frequency by selecting the one with the biggest phase margin.

3.2 Link position control

A PD controller addresses the link position control by computing the target motor speed signal $\dot{\theta}_t$. The controller is described by the following transfer function:

$$C_p(s) = K_{p,p} + \frac{K_{d,p}s}{T_{f,p}s + 1} \quad (13)$$

where $K_{p,p}$ is the proportional gain, $K_{d,p}$ is the derivative gain, and $T_{f,p}$ is the filter time constant. Controller $C_p(s)$ acts on the process made by the secondary loop $P_{\dot{\theta}_t,q}(\hat{\omega})$ as shown in Figure 2. The target motor speed signal $\dot{\theta}_t$ is given by the controller output plus a feedforward action equal to the velocity profile provided by the link motion planner. Integral action is not employed since $P_{\dot{\theta}_t,q}(\hat{\omega})$ has a pole at the origin and external disturbances are managed by the secondary loop.

The controller parameters can be rewritten by following (6) as

$$\hat{K}_{p,p} = K_{p,p}\sqrt{\frac{J_m}{k}}, \; K_{p,p} = \hat{K}_{p,v}\sqrt{\frac{k}{J_m}},$$
$$\hat{K}_{d,p} = K_{d,p}, \qquad K_{d,p} = \hat{K}_{d,p}, \quad (14)$$
$$\hat{T}_{f,p} = T_{f,p}\sqrt{\frac{k}{J_m}}, \quad T_{f,v} = \hat{T}_{f,p}\sqrt{\frac{J_m}{k}},$$

As in Section 3.1, the controller parameters are computed by solving the following optimization problem:

$$\min(\hat{\omega}_{c,p} - \hat{\omega}_{d,p})^2 - \lambda_p \phi_m$$

$$\text{subject to:} \begin{cases} \phi_m \geq \phi_{m,min} \\ M_s \leq M_{s,max} \\ |L_p(\hat{\omega})| \leq L_{h,p,max}, \text{ if } \hat{\omega} \geq \hat{\omega}_h \\ |L_p(\hat{\omega})| \geq L_{l,p,min}, \text{ if } \hat{\omega} \leq \hat{\omega}_l \end{cases} \quad (15)$$

where $\hat{\omega}_{c,v}$ and $\hat{\omega}_{d,v}$ are, respectively, the cutoff frequency and its desired value, $L_p(\hat{\omega}) = C_v(\hat{\omega})P_{\dot{\theta}_t,q}(\hat{\omega}))$ is the loop transfer function, $L_{h,p,max}$ is the maximum allowed value of $|L(\hat{\omega})|$ for frequencies greater than $\hat{\omega}_h$, while $L_{l,p,min}$ is the minimum allowed value for frequencies lower than $\hat{\omega}_l$ and $\lambda_v > 0$ is a weighting factor. In the tuning procedure, those values have been set equal to:

$$\begin{aligned} L_{h,p,max} &= 40dB, \quad \hat{\omega}_h = 100\hat{\omega}_d, \\ L_{l,p,min} &= 20dB, \quad \hat{\omega}_h = 0.01\hat{\omega}_d, \\ M_{s,max} &= 1.4, \quad \phi_{m,min} = 60° \\ \lambda_p &= 10^{-2} \end{aligned} \quad (16)$$

3.3 Tuning rules

During the robot working activities, the link inertia can significantly change, and therefore a gain scheduling approach is highly recommended. However, solving (11) and (15) online is not possible due to computational burdens. For this reason, the development of an approximate solution by means of tuning rules has been performed, in order to allow the online computation of the robust controller for a given value of J_l. The motor velocity controller tuning is performed by imposing the desired cutoff frequency to be part of the set $\hat{\omega}_{d,v} \in \{3,4,5,6,7,8,9,10\}$. In order to find the tuning rules, the optimization problem (11) has been repeated 2000 times by varying $\hat{h}$ in the interval [0.01, 0.5], $\hat{f}_m$ in the interval [0.0, 0.5], and $\hat{J}_m$ in the interval [0.5, 2] for each value of cutoff frequencies.

The resulting controllers parameters are approximated by means of the following tuning rules:

Table 1. Matrices coeffients of the motor velocity tuning rules when $\hat{\omega}_{d,v} = 3$

$M_{\hat{K}_p}$	2.531878	-0.187629	0.766849	0.176141	2.369994
	0.065366	0.590771	-1.589730	0.125980	-2.663157
	0.000677	-0.295008	0.763627	-0.124333	0.946668
$M_{\hat{K}_i}$	0.001504	3.001502	-0.006152	-0.000658	-0.009293
	0.051657	-0.256998	0.367284	-0.000003	0.009802
	0.010598	-0.028327	0.025340	0.000178	-0.003194

Table 2. Matrices coeffients of the motor velocity tuning rules when $\hat{\omega}_{d,v} = 4$

$M_{\hat{K}_p}$	3.708948	-0.108430	0.377811	0.037026	1.437171
	0.011955	0.260642	-0.653636	0.130305	-1.496274
	0.003181	-0.116833	0.292964	-0.071785	0.498541
$M_{\hat{K}_i}$	-0.003161	4.029311	-0.046981	-0.000382	-0.009993
	0.127712	-0.628493	0.890955	-0.000331	0.009936
	0.015017	-0.008518	-0.026994	0.000229	-0.003068

Table 3. Matrices coeffients of the motor velocity tuning rules when $\hat{\omega}_{d,v} = 5$

$M_{\hat{K}_p}$	4.791588	-0.113563	0.302272	0.032533	0.976789
	-0.003609	0.189006	-0.436630	0.068670	-0.936631
	0.003717	-0.074892	0.180993	-0.036597	0.298819
$M_{\hat{K}_i}$	-0.009775	5.061989	-0.088155	-0.000461	-0.010757
	0.249213	-1.201760	1.679001	-0.000247	0.010181
	0.014515	0.064108	-0.166778	0.000201	-0.003044

Table 4. Matrices coeffients of the motor velocity tuning rules when $\hat{\omega}_{d,v} = 6$

$M_{\hat{K}_p}$	5.850311	-0.174389	0.379250	0.000514	0.796468
	-0.025962	0.249436	-0.541724	0.102136	-0.787528
	0.010387	-0.094186	0.217908	-0.049836	0.261223
$M_{\hat{K}_i}$	-0.015671	6.076707	-0.089640	-0.000315	-0.012242
	0.418010	-1.954373	2.674216	-0.000646	0.011784
	0.007221	0.196555	-0.397502	0.000421	-0.003593

Table 5. Matrices coeffients of the motor velocity tuning rules when $\hat{\omega}_{d,v} = 7$

$M_{\hat{K}_p}$	6.897957	-0.263959	0.537100	-0.048779	0.747911
	-0.054282	0.386998	-0.835283	0.186529	-0.833085
	0.020995	-0.150384	0.344335	-0.088107	0.301129
$M_{\hat{K}_i}$	-0.017312	7.046733	-0.007167	0.000191	-0.014580
	0.631822	-2.839686	3.784653	-0.001803	0.015161
	-0.007112	0.383480	-0.702280	0.001026	-0.004937

$$\hat{K}_p = \begin{bmatrix} 1 & \hat{f}_m & \hat{f}_m^2 & \hat{h} & \hat{h}^2 \end{bmatrix} M_{\hat{K}_p} \begin{bmatrix} 1 \\ \hat{J}_l \\ \hat{J}_l^2 \end{bmatrix}$$
$$\hat{K}_i = \begin{bmatrix} 1 & \hat{f}_m & \hat{f}_m^2 & \hat{h} & \hat{h}^2 \end{bmatrix} M_{\hat{K}_i} \begin{bmatrix} 1 \\ \hat{J}_l \\ \hat{J}_l^2 \end{bmatrix} \quad (17)$$

The resulting values for each $\hat{\omega}_{d,v}$ are in Tables 1-8. For all the values of $\hat{\omega}_{d,v}$ the maximum sensitivity is much smaller than 1.4, as shown in Figure 6, which demonstrates the effectiveness of the tuning rules to ensure the required robustness.

The link position controller tuning rules are also computed by solving 2000 times the optimization problem (15) by using the motor velocity tuning rules with $\hat{\omega}_{d,v} = 3$, even if it can be used also with faster secondary controlled systems. The primary loop cutoff frequency is set to $\hat{\omega}_{d,p} = 1$ but, differently to the secondary loop case, the constraint $M_s = 1.4$ limits the bandwidth in the range [0.3,

Table 6. Matrices coeffients of the motor veloc-
ity tuning rules when $\hat{\omega}_{d,v} = 8$

$M_{\hat{K}_p}$	7.946372	-0.410546	0.836845	-0.142072	0.832658
	-0.101432	0.656619	-1.444846	0.373792	-1.122394
	0.040938	-0.269486	0.621562	-0.175203	0.448979
$M_{\hat{K}_i}$	-0.011250	7.948294	0.195722	0.001579	-0.018751
	0.886549	-3.804287	4.914911	-0.004912	0.022654
	-0.027762	0.613100	-1.055465	0.002601	-0.008212

Table 7. Matrices coeffients of the motor veloc-
ity tuning rules when $\hat{\omega}_{d,v} = 9$

$M_{\hat{K}_p}$	8.996517	-0.605634	1.256875	-0.259264	0.988444
	-0.163220	1.035979	-2.316475	0.619581	-1.544295
	0.068099	-0.440535	1.022770	-0.291915	0.659486
$M_{\hat{K}_i}$	0.005449	8.763461	0.543840	0.003918	-0.024746
	1.177551	-4.797556	5.980280	-0.010142	0.034360
	-0.053453	0.871060	-1.428947	0.005280	-0.013569

Table 8. Matrices coeffients of the motor veloc-
ity tuning rules when $\hat{\omega}_{d,v} = 10$

$M_{\hat{K}_p}$	10.058496	-0.854067	1.833301	-0.489032	1.374578
	-0.257929	1.543944	-3.549797	1.106527	-2.438658
	0.111149	-0.676386	1.604185	-0.522677	1.091335
$M_{\hat{K}_i}$	0.034812	9.481141	1.048431	0.009575	-0.037039
	1.500984	-5.778026	6.918657	-0.022352	0.059535
	-0.082965	1.143977	-1.799310	0.011330	-0.025308
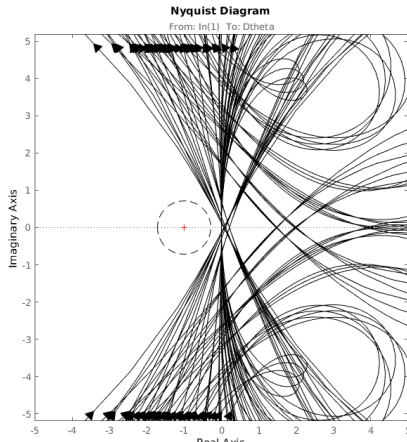
Fig. 6. Nyquist plot of the motor velocity open loop
transfer function ($\hat{\omega}_{d,v} = 10$). The dashed circle
indicates the value $M_s = 1.4$.

0.6] depending on the values of $\hat{h}$, $\hat{f}_m$, and $\hat{J}_l$. Thus, the
proposed tuning rules provide the fastest primary loop.
The tuning rules are expressed by means of the following
equation:

$$\hat{K}_p = \begin{bmatrix} 1 & \hat{f}_m & \hat{f}_m^2 & \hat{h} & \hat{h}^2 \end{bmatrix} M_{\hat{K}_p} \begin{bmatrix} 1 \\ \hat{J}_l \\ \hat{J}_l^2 \\ 1 \\ \hat{J}_l \\ \hat{J}_l^2 \end{bmatrix}$$

$$\hat{K}_d = \begin{bmatrix} 1 & \hat{f}_m & \hat{f}_m^2 & \hat{h} & \hat{h}^2 \end{bmatrix} M_{\hat{K}_d} \begin{bmatrix} 1 \\ \hat{J}_l \\ \hat{J}_l^2 \\ 1 \\ \hat{J}_l \\ \hat{J}_l^2 \end{bmatrix} \quad (18)$$

$$\hat{T}_f = \frac{1}{5}$$

The resulting values are in Table 9.
Figure 7 shows that the maximum sensitivity is limited to
1.4 demonstrating the effectiveness of the tuning rules to
ensure the required robustness.

Table 9. Matrices coeffients of the link position
tuning rules when $\hat{\omega}_{d,p} = 1$

$M_{\hat{K}_p}$	0.063902	0.152822	-0.281618	-0.057527	2.330662
	0.035825	-0.212446	0.385927	0.071206	-2.876210
	-0.019325	0.069888	-0.132506	0.059622	0.735524
$M_{\hat{K}_d}$	0.026688	-0.275392	0.682902	-0.568180	2.708334
	-0.042239	0.780534	-1.706131	0.081026	-1.507766
	0.026225	-0.414427	0.850398	0.176679	0.063388
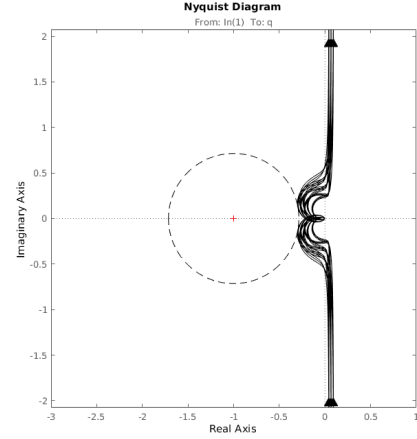
Fig. 7. Nyquist plot of the link position open loop transfer
function ($\hat{\omega}_{d,v} = 10$ and $\hat{\omega}_{d,p} = 1$). The dashed circle
indicates the value $M_s = 1.4$.

Fig. 8. FourByThree Series Elastic Actuated robot

Parameter	Value	Reduced value
J_m	0.883024 [kgm^2]	[-]
k	735.343764 [Nm/rad]	[-]
h	7.8928 [Nm/(rad/s)]	0.301
f_m	6.966257 [Nm/(rad/s)]	0.27
J_l (no payload)	0.650 [kgm^2]	0.736

Table 10. Dynamics parameters of Joint 1

4. EXPERIMENTAL RESULTS

The proposed tuning rules are tested on a three degree-of-
freedom series elastic actuated robot, designed as a part of
the FourByThree European project (FourByThree, 2018).
The actuators are composed by a brushless DC motor,
an harmonic driver and an elastic element made by a
series of coil springs. The actuator has two encoders: one
measures the motor position after the harmonic drive while
the second measures the angle after the spring element.
The current loop is implemented inside a FPGA board
and it is considered as a unitary gain for the position
and velocity controllers. The torque reference signal is sent
to the FPGA board by using the ROS operating system
framework (ROS, 2018).
Joint 1 has been used to show the effectiveness of the
proposed method during a trajectory tracking task. The
dynamics parameters of the robot are in Table 10.
Moreover, there is a static friction of $C_m = 2.3$ [Nm]
and a backlash of 0.015 [rad] (around 1 [deg]) which are
considered as model mismatches, as well as the coupling
effect caused by the other links.
The control performance are tested by means of two
trajectories. In particular, a trapezoidal motion profile
from position 0 [rad] to 1.5708 [rad] followed by another
trapezoidal motion profile from 1.5708 [rad] to 0 [rad]

Parameter	Value	Reduced value
J_l (no payload)	0.650 [kgm^2]	0.736
J_l (m= 0.5 [kg])	0.740 [kgm^2]	0.8385
J_l (m= 1 [kg])	0.786 [kgm^2]	0.890
J_l (m= 2 [kg])	0.924 [kgm^2]	1.047
J_l (m= 5 [kg])	1.514 [kgm^2]	1.714

Table 11. Link inertia values with disk payloads.

Payload	$|\bar{e}|_p$	$|\bar{e}|_v$	c_e
J_l (no payload)	0.0014 [rad]	0.0548 [rad/s]	0.3055 [Nm]
J_l (m= 0.5 [kg])	0.0019 [rad]	0.0471 [rad/s]	0.3073 [Nm]
J_l (m= 1 [kg])	0.0018 [rad]	0.0720 [rad/s]	0.4243 [Nm]
J_l (m= 2 [kg])	0.0012 [rad]	0.0498 [rad/s]	0.3466 [Nm]
J_l (m= 5 [kg])	0.0020 [rad]	0.0648 [rad/s]	0.3902 [Nm]

Table 12. performance indexes for the different J_l values.
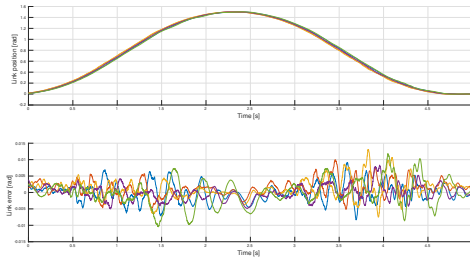
Fig. 9. Link position and error trends with different J_l values. Blue line: no payload. Magenta line: 0.5 [kg] payload. Ocher line: 1 [kg] payload. Violet line: 2 [kg] payload. Green line: 5 [kg] payload.

has been considered. The motor velocity cutoff frequency has been chosen equal to $\hat{\omega}_{d,p} = 3$, which corresponds to $\omega_{d,p} = 86.5735$ [rad/s]. In order to demonstrate the robustness of the controller, four different disk payloads have been attached to the robot flange, changing J_l as shown in Table 11.

For each test, the performance are evaluated by computing the link position and the motor velocity mean absolute errors (respectively, $|\bar{e}|_p$ and $|\bar{e}|_v$) and the control effort c_e defined as

$$c_e = \frac{1}{T} \int_{t=0}^{T} |\Delta\tau| dt$$

The obtained values are in Table 12, while Figure 9 shows the position and the torque trends for each J_l values. It is possible to note the effectiveness of the proposed method to follow the required set-point signal in presence of an unknown payload. In fact, the mean absolute errors are limited also in the most critical situation (namely, the 5 [kg] payload case).

5. CONCLUSIONS

Robust tuning rules for Series Elastic Actuator control have been presented. The tuning rules are designed for a PD-PI cascade control and allow the online computation of the robust control parameters for each value of the link inertia. Experimental results show the effectiveness of the methodology on a three degree-of-freedom series elastic actuated robot.

ACKNOWLEDGEMENTS

REFERENCES

Åström, K.J. and Hägglund, T. (2004). Revisiting the Ziegler-Nichols step response method for PID control. *Journal of Process Control*, 14(6), 635–650. doi:10.1016/j.jprocont.2004.01.002.

Calanca, A. and Fiorini, P. (2017). Impedance control of series elastic actuators based on well-defined force dynamics. *Robotics and Autonomous Systems*, 96, 81–92. doi:10.1016/j.robot.2017.06.013.

Calanca, A., Muradore, R., and Fiorini, P. (2017). Impedance control of series elastic actuators: Passivity and acceleration-based control. *Mechatronics*, 47, 37–48. doi:10.1016/j.mechatronics.2017.08.010.

Dos Santos, W.M. and Siqueira, A.A.G. (2014). *Impedance control of a rotary series elastic actuator for knee rehabilitation*, volume 19. IFAC. doi:10.1109/ICAR.2013.6766567.

FourByThree (2018). Fourbythree project homepage. http://http://fourbythree.eu/. Accessed: 2018-01-31.

Guiochet, J., Machin, M., and Waeselynck, H. (2017). Safety-critical advanced robots: A survey. *Robotics and Autonomous Systems*, 94, 43–52. doi:https://doi.org/10.1016/j.robot.2017.04.004.

Maleki, S., Parsa, A., and Ahmadabadi, M.N. (2016). Feed-forward learning with frequency adaptation towards the control of series elastic actuators. In *2016 4th International Conference on Robotics and Mechatronics (ICROM)*, 196–201. doi:10.1109/ICRoM.2016.7886846.

Maurtua, I., Pedrocchi, N., Orlandini, A., d. G. Fernndez, J., Vogel, C., Geenen, A., Althoefer, K., and Shafti, A. (2016). Fourbythree: Imagine humans and robots working hand in hand. In *2016 IEEE 21st International Conference on Emerging Technologies and Factory Automation (ETFA)*, 1–8. doi:10.1109/ETFA.2016.7733583.

Misgeld, B.J., Hewing, L., Liu, L., and Leonhardt, S. (2017). Robust gain-scheduled control of variable stiffness actuators. *IFAC-PapersOnLine*, 50(1), 8804–8809. doi:10.1016/j.ifacol.2017.08.1535.

Paine, N., Oh, S., and Sentis, L. (2014). Design and control considerations for high-performance series elastic actuators. *IEEE/ASME Transactions on Mechatronics*, 19(3), 1080–1091. doi:10.1109/TMECH.2013.2270435.

Ragonesi, D., Agrawal, S., Sample, W., and Rahman, T. (2011). Series elastic actuator control of a powered exoskeleton. In *2011 Annual International Conference of the IEEE Engineering in Medicine and Biology Society*, 3515–3518. doi:10.1109/IEMBS.2011.6090583.

ROS (2018). ROS homepage. http://wwww.ros.org. Accessed: 2018-01-31.

Simoni, L., Beschi, M., Legnani, G., and Visioli, A. (2017). Modelling the temperature in joint friction of industrial manipulators. *Robotica*, 122. doi:10.1017/S0263574717000509.

Verstraten, T., Beckerle, P., Furnémont, R., Mathijssen, G., Vanderborght, B., and Lefeber, D. (2016). Series and Parallel Elastic Actuation: Impact of natural dynamics on power and energy consumption. *Mechanism and Machine Theory*, 102, 232–246. doi:https://doi.org/10.1016/j.mechmachtheory.2016.04.004.